CHALMERS
UNIVERSITY OF TECHNOLOGY

Synchronization and Channel Estimation in Massive MIMO Systems

Master's thesis in Communication Engineering

Jianing Bai

Department of Signals and Systems
CHALMERS UNIVERSITY OF TECHNOLOGY
Gothenburg, Sweden 2016

MASTER'S THESIS IN COMMUNICATIONA ENGINEERING

Synchronization and Channel Estimation in Massive MIMO Systems

[Abstract]

Jianing Bai

Department of Signals and Systems
CHALMERS UNIVERSITY OF TECHNOLOGY
Göteborg, Sweden 2016

Synchronization and Channel Estimation in Massive MIMO Systems
[Abstract]
Jianing Bai

Master's Thesis EX053/2016
Department of Signals and Systems
Chalmers University of Technology
SE-412 96 Göteborg
Sweden
Telephone: + 46 (0)31-772 1000

Department of Signals and Systems
Göteborg, Sweden 2016-08-15

Synchronization and Channel Estimation in Massive MIMO Systems
Master's thesis in Master's Communication Engineering
Jianing Bai
Department of Signals and Systems
Chalmers University of Technology

Abstract

Massive multiple-input multiple-output (MIMO) is a strong candidate for the fifth generation (5G) communications system for its high data rate and link reliability. Combining the massive MIMO with orthogonal frequency division multiplexing (OFDM) technique will increase the robustness of the system against the delay spread in the multipath channel. However, OFDM systems are sensitive to frequency synchronization errors, which degrade the system performance significantly. In addition, OFDM systems also suffer from high peak to average power ratio (PAPR). Hence we also consider single carrier system (SC), which has a much lower PAPR.

Specifically, in this thesis, we studied symbol synchronization for correcting time delays for massive MIMO systems with SC. We implemented symbol synchronization for the MIMO downlink case (each user performs symbol synchronization). It is found that the Gardner's algorithm can be readily applied for the massive MIMO system for symbol synchronization.

For OFDM-based massive MIMO systems, both channel estimation and frequency synchronization are considered. For feasible channel estimation for the massive MIMO system, the time-division duplex (TDD) is assumed, in which case, the standard least-square (LS) channel estimation is applied in the uplink (UL), and the estimated channel is then used for MIMO precoding in the downlink (DL). The OFDM system is sensitive to the carrier frequency offset (CFO). We use pilot-based CFO estimation (instead of blind frequency synchronization) to ensure good performance of the frequency synchronization. To avoid the high complexity of joint estimation of the CFOs of all the users at the base station, we assume that each user estimates its CFO during the DL and adjusts its transmission accordingly in the UL. It is shown that the CFO estimation of the MIMO system has similar performance as that of the single-input single-output system.

Key words: Channel estimation, carrier frequency offset, frequency synchronization, MIMO, symbol synchronization.

Contents

Abstract I
Contents II
Acknowledgements IV
Notation V
1 Introduction 1
2 Massive MIMO System Model 2
2.1 Modulation 2
2.2 Precoding 2
2.2.1 MRT 2
2.2.2 ZF 3
2.2.3 MMSE 3
2.3 Pulse Shaping 4
2.4 I/Q Imbalance 4
2.5 Phase Noise 5
2.6 Matched Filter 5
3 Symbol Synchronization 6
3.1 Timing Offset and Recovery 6
3.2 Gardner's Method for Timing Recovery 7
3.2.1 Interpolator 9
3.2.2 Timing Error Detector 10
3.2.3 Loop Filter 11
3.2.4 NCO 12
3.3 Simulations 12
3.3.1 SISO 13
3.3.2 MIMO 15
4 Channel Estimation 18
4.1 Multipath Fading Channel 18
4.2 OFDM 19
4.3 LS Channel Estimation 20
4.3.1 SISO 20
4.3.2 MIMO 20
4.4 Simulations 23
4.4.1 Performance of Channel Estimation 23

4.4.2 Equalization performance 25
5 Frequency Synchronization 27
5.1 CFO Estimation 27
5.2 Simulation 29
5.2.1 SISO 29
5.2.2 MIMO 30
6 Conclusion 32
7 References 33

Acknowledgements

First of all, I would like to thank my supervisor and examiner, Prof. Thomas Eriksson, for offering me such an interesting topic for my Master thesis. I am also grateful for his insightful and helpful guidance's and kind encouragement throughout this thesis.

I would also like to thank my secondary supervisor, Dhecha Nopchinda, for his discussions and comments in our routine meetings.

Last but not least, I thank my husband and my son for their love and support during my study.

Göteborg May 2016-08-15

Jianing Bai

Notation

$(\bullet)^*$	Complex conjugate
$(\bullet)^T$	Transpose
$(\bullet)^H$	Hermitian
$(\bullet)^+$	Pseudo-inverse
$\|(\cdot)\|^2$	2-norm of the argument
$\angle(\bullet)$	Angle of argument
x	Scalar
$\mathbf{x}$	Column vector
$\mathbf{X}$	Matrix
I	Identity matrix
j	$\sqrt{-1}$
H	Channel transfer function
G	Precoding matrix
a_k	Transmitted symbols
$v(t)$	Pulse filter
β	Roll-off factor
A	Amplitude
f_c	Carrier frequency
$\varphi(t)$	Phase noise
τ	Time delay
K_1	Proportional gain
K_2	Integrator gain
b_l	Filter coefficients
$B_n T_s$	Normalized loop bandwidth
K_P	Detector gain
ξ	Damping factor
$*$	Convolution

1 Introduction

Massive MIMO usually involves hundreds of (or even more) antennas at the base station (BS) to serve a number of users that are much smaller than the number of BS antennas. The massive MIMO system can effectively increase the data rate, improve the reliability and the energy efficiency, and reduce the spatial interferences compared with conventional point-to-point MIMO [1]. Therefore, it is considered as a strong candidate for 5G communications.

However, the great advantages of the massive MIMO system are not without any cost. For example, the large number of BS antennas makes the downlink (DL) channel estimation a challenging task. As a result, the time-division duplex (TDD) is usually assumed so that the BS can use the estimated channel during the uplink (UL) transmission for DL precoding. In addition, each of the BS antennas requires a radio frequency (RF) chain, which can increase the system cost drastically. Therefore, the "dirty RF" or hardware impairments on the massive MIMO system and the feasible schemes for compensating these impairments are important research topics that deserve more attention.

The dirty RF includes phase noises and carrier frequency offsets (CFOs) of the oscillators, the I/Q imbalances of the gains and phases of the I/Q channels in the circuitry, the nonlinearity of the power amplifier, etc. While it is impossible to address all these impairments in this Master thesis, we focus on the frequency synchronization for the CFO compensation, channel estimation, and symbol synchronization for compensating the unknown delays in the propagation channels.

The rest of the thesis is organized as follow: Chapter 2 gives an overview of the components, functional modules, and hardware impairments of the massive MIMO system. The symbol synchronization is studied in Chapter 3 for the SC-based massive MIMO system. Chapter 4 focus on channel estimation of the OFDM-based massive MIMO system. Chapter 5 deals with CFO estimation and frequency synchronization of the OFDM-based massive MIMO system. Chapter 6 concludes the thesis.

2 Massive MIMO System Model

Fig. 2.1 shows the block diagram of the massive MIMO system. Each functional module of the massive MIMO systems is described next.

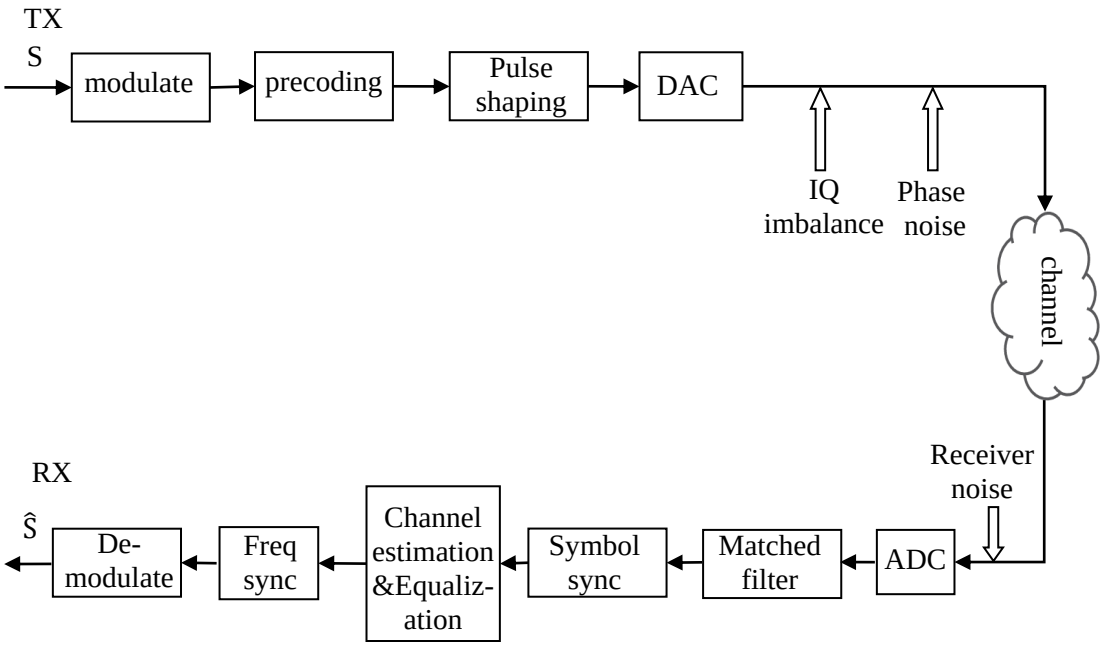

Figure 2.1 Block diagram of the massive MIMO system.

2.1 Modulation

We can choose different modulation orders of quadrature amplitude modulation (QAM), e.g. 16-QAM. The transmitted symbol is given as $\mathbf{X} = \begin{bmatrix} \mathbf{x}_1 & \dots & \mathbf{x}_K \end{bmatrix}$ where $\mathbf{x}_k = \begin{bmatrix} x_k(0) & \dots & x_k(N-1) \end{bmatrix}^T$ with N denoting the number for QAM symbols, x_k, in one transmission block. We assume the channel stays constant within a block (i.e. N symbols). Note that, for notational convenience, we have omitted the block index.

2.2 Precoding

Precoding is a transmission technique to support multi-stream transmission. Using the full channel state information (CSI) at the transmitter, precoding can mitigate the interference between data streams, and allocate resources optimally [2]. Various precoding methods exist, e.g. zero-forcing (ZF), minimum mean squared error (MMSE), maximum ratio transmission (MRT), etc.

2.2.1 MRT

The MRT precoding matrix $\mathbf{G}$ is $\mathbf{G} = \mathbf{H}^H$ [3], where $\mathbf{H}$ is the $M \times K$ channel matrix between the M BS antennas and the K users (each equipped with single antenna). It is

assumed that the channel stays constant within each block. Hence, the precoded signals can be expressed as

$$\mathbf{X}_{\mathbf{pre}} = \mathbf{XG} = \mathbf{XH}^{H}. \tag{2.1}$$

The received signals at the K users can be written as

$$\mathbf{Y} = \mathbf{X}_{\mathbf{pre}}\mathbf{H} + \mathbf{W} = \mathbf{XH}^{H}\mathbf{H} + \mathbf{W} \tag{2.2}$$

where $\mathbf{W}$ is a $N \times K$ matrix consists of additive white Gaussian noises (AWGN) over the N symbols in the time domain and K users in the spatial domain. As can be seen from (2.2), the MRT precoding aims at maximizing the signal-to-noise-ratio (SNR) at each user while ignoring the interferences between different users. In general, MRT precoding results in worse performance as compared with ZF and MMSE precoding. Nevertheless, in the low SNR regime (where the interference power falls below the noise power), the MRT precoding can outperform ZF precoding and becomes favorable due to its low computational complexity [3].

2.2.2 ZF

For ZF precoding, $\mathbf{G}$ is the pseudo-inverse of $\mathbf{H}$ [3].

$$\mathbf{G} = \mathbf{H}^{+} = (\mathbf{H}^{\mathbf{H}}\mathbf{H})^{-1}\mathbf{H}^{\mathbf{H}}. \tag{2.3}$$

The precoded signals can be expressed as

$$\mathbf{X}_{\mathbf{pre}} = \mathbf{XG} = \mathbf{XH}^{+}. \tag{2.4}$$

The received signals at the K users can be written as

$$\mathbf{Y} = \mathbf{X}_{\mathbf{pre}}\mathbf{H} + \mathbf{W} = \mathbf{XH}^{+}\mathbf{H} + \mathbf{W} = \mathbf{X} + \mathbf{W}. \tag{2.5}$$

As can be seen from (2.5), the ZF precoding completely removes interferences between different users. One drawback of the ZF precoding, compared with the MRT, is the high computational complexity associated with the pseudo-inverse calculation of the large matrix $\mathbf{H}$. Nevertheless, its complexity is smaller than the MMSE precoding. In this thesis, without specifications, the ZF precoding is assumed for simulations.

2.2.3 MMSE

For MMSE precoding, $\mathbf{G}$ is $\mathbf{G} = \left(\mathbf{H}^{H}\mathbf{H} + \frac{1}{\rho}\mathbf{I}\right)^{-1}\mathbf{H}^{H}$ [3], where ρ is the ratio of transmitted symbol energy to noise spectral density. The MMSE precoding is a trade-off between noise and interference. It outperforms ZF precoding (has similar performance as MRT precoding) at low SNR and outperforms MRT precoding (has similar performance as ZF precoding) at high SNR. In addition, compared with ZF precoding, the MMSE precoding is more robust to correlations between users, which may arise when users are closely spaced or share the common scatters [3].

2.3 Pulse Shaping

Pulse shaping is usually used to compress the spectrum of the transmitted signal while avoiding inter-symbol interference (ISI).

The transmitted signal can be represented as

$$s(t) = \sum_{k=0}^{\infty} a_k v(t - kT_s) \tag{2.5}$$

where a_k is the transmitted symbols and $v(t)$ is the pulse filter. The square root raised cosine (RRC) pulse is usually chosen as the pulse filter. The RRC pulse is used in this thesis for it is used in most practical transceivers [4]. The RRC pulse can be regarded by splitting the RC filter into two RRC filters, and put one in the transmitter to do the pulse shaping, and the other RRC in the receiver to mitigate the ISI. The impulse response of RRC filter is shown in the Fig. 2.2. One important parameter is the roll off factor β, which measure the bandwidth of the filer occupied beyond the Nyquist bandwidth [5].

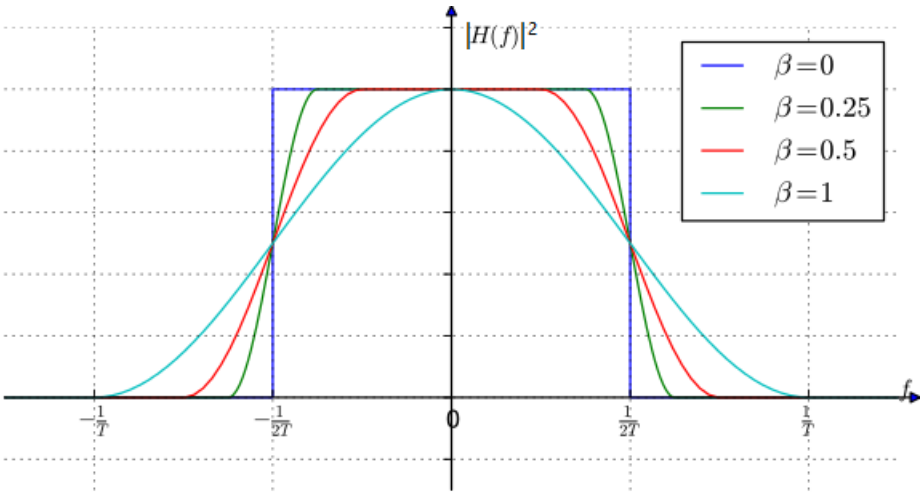

Figure 2.2 The impulse response of a RRC filter with different roll-off factors [5].

2.4 I/Q Imbalance

I/Q imbalance is caused by the mismatches in phases and gains between the in-phase (I) and quadrature (Q) signal branches. The I and Q branches are supposed to have 90 degree phase difference and equal gain. However, in the analog circuit, phase shifter does not provide exactly 90-degree phase difference between the IQ branches; and the gains of the IQ branches are not exactly the same [6]. In this thesis, we ignore the I/Q imbalance problem. Since it's often involved in the wireless communication, we introduce this concept briefly.

2.5 Phase Noise

An ideal oscillator generates a pure sine wave $A\cos(2\pi f_c t)$, which can be represented as a single spectral line in frequency domain. However, a real oscillator always has some random phase fluctuations. $v(t) = A\cos(2\pi f_c t + \varphi(t))$. In frequency domain, this is represented as spread of spectral lines, spreading the power to adjacent frequencies. The phase noise of a free-running oscillator is usually modeled by a Wiener process. In practice, a phase lock loop (PLL) is usually used to reduce the phase noise of the free-running oscillator [7].

2.6 Matched Filter

Usually, when a pulse shaping filter is applied at the transmitter side, a matched filter will be needed at the receiver side to for optimal SNR performance. For a given pulse shaping filter $v(t)$, the matched filter can be constructed as $h_R(t) = v(-t)$.

In this thesis, we focus on the symbol synchronization, frequency synchronization, and channel estimation, respectively.

3 Symbol Synchronization

In this chapter, we deal with the timing offset for SC systems. We first present the symbol synchronization for the single-input single-output (SISO) system and then extend it to the massive MIMO system.

3.1 Timing Offset and Recovery

The symbol synchronization, also known as timing recovery, is required in asynchronous (wireless) communications system. In a digital modem, to perform demodulation, the receiver needs to know the arrival time of the transmitted symbols and sampling periodically at the symbol rate of the incoming signal to recover the received signal. The transmitter and receiver clocks are in general very accurate. But there are some perturbations caused by, e.g., (fractional) channel delay, clock jitter and mismatch, etc. The received signal can be expressed as

$$r(t) = \sum_{k=0}^{K-1} a_k v(t - kT - \tau_k) + \omega(t) \tag{3.1}$$

Where a_k is the transmitted symbols, K is the frame length, $v(t)$ is pulse shaping filter, T is the symbol period, $\omega(t)$ is AWGN noise, and τ_k is the unknown timing offset. The receiver needs to estimate the delay τ_k in order to sample the received signal at the optimal instants $(kT + \tau_k)$ [8]. Otherwise, there will be inter-symbol interference (ISI), which can significantly degrade the performance of the system [9]. The role of the symbol synchronization is to synchronize the receiver clock with the symbol rate in order to obtain samples at the correct instances.

Symbol synchronization plays an important role in MIMO systems. Since in MIMO systems, the receiver needs to recapture multiple data streams via multipath. Incorrect sampling time will cause not only ISI within a spatial stream but also inter-stream interferences (i.e., interferences between different data streams) [10]. This will degrade the MIMO performance severely. Therefore, MIMO systems are more sensitive to symbol synchronization errors compared with SISO systems [11].

To solve this problem, we can adjust the sampling clock with a mechanism controller, or control the sampling clock by digital techniques. But in some cases, the local clock is independent of the symbol timing controller and cannot be adjusted, as shown in Fig. 3.1. In this case, we need to find digital techniques to do the timing recovery on the signal without changing the sampling clock.

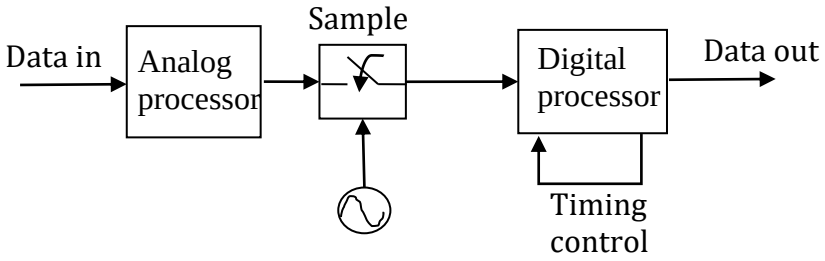

Figure 3.1 Timing recovery method [12].

3.2 Gardner's Method for Timing Recovery

The actual role of the symbol synchronization is to produce the correct strobe values by interpolating the non-synchronized samples. Different methods exist for symbol synchronizations. For SC systems, the Gardner's symbol synchronization [12]-[14] is perhaps the most popular timing recovery method. The Gardner's method is a non-data-aided (NDA) method, which does not depend on known or detected symbols. It is widely used in timing recovery schemes for its simple structure, and it treats carrier signals as baseband signals [12]. Compared with the decision-directed algorithm, Gardner's algorithm is independent of carrier phases, so that both passband and baseband signals can be processed using the Gardner's method. As a result, in this thesis, we use the Gardner's method for timing recovery for the SC-based SISO and MIMO systems.

The Gardner's algorithm needs at least two samples per symbol. We illustrate the Gardner's algorithm assuming an oversampling factor of two in this section (whereas the algorithm can be readily applied to systems with larger oversampling factors). The timing error detector (TED) is based on the delay difference between the two samples to find the correct sampling instances. The difference between two samples in each symbol can be expressed as

$$x_d(t) = x(t) - x(t - T/2) \tag{3.2}$$

Then pass the stream $x_d(t)$ through a rectifier to regenerate a clock wave [12]

$$x_d^2(t) = x^2(t) + x^2(t - T/2) - 2x(t)x(t - T/2) \tag{3.3}$$

If the early sampling time for the r-th strobe is at $t = rT + \tau$, where τ is the delay time, we get

$$\begin{aligned} E(r) &= x_d^2(rT + \tau) \\ &= x^2(rT + \tau) + x^2\{(r - 1/2)T + \tau\} - 2x(rT + \tau)x\{(r - 1/2)T + \tau\} \end{aligned} \tag{3.4}$$

And the late sampling time for the (r-1)-th at $t = rT + \tau - T/2$ can be expressed as

$$L(r-1) = x_d^2\{(r-1/2)T+\tau\}$$
$$= x^2\{(r-1/2)T+\tau\} + x^2\{(r-1)T+\tau\} - 2x\{(r-1/2)T+\tau\}\,x\{(r-1)T+\tau\} \quad (3.5)$$

Subtract $E(r)$ and $L(r-1)$, we get

$$u_t(r) = L(r-1) - E(r)$$
$$= x^2\{(r-1)T+\tau\} - x^2\{rT+\tau\} + 2x\{(r-1/2)T+\tau\}\{x(rT+\tau) - x\{(r-1)T+\tau\}\} \quad (3.6)$$

Considering the average value over many samples, the first two terms in (3.6) are canceled. The remaining term is

$$u_t(r) = x\{(r-1/2)T+\tau\}\{x(rT+\tau) - x\{(r-1)T+\tau\}\} \quad (3.7)$$

When the delay time τ equals zero, the timing-detector algorithm can be expressed as

$$u_t(r) = x(r-1/2)\{x(r) - x(r-1)\} \quad (3.8)$$

To estimate timing error for both I and Q channels, we compute each channel by using (3.8) and added them up

$$u_t(r) = y_I(r-1/2)\{y_I(r) - y_I(r-1)\} + y_Q(r-1/2)\{y_Q(r) - y_Q(r-1)\} \quad (3.9)$$

The Gardner algorithm can be used for synchronize both baseband signal and passband signals with approximately 40 to 100 percent excess bandwidth, which means the roll off factor of the filter pulse used for pulse shaping should be larger than 0.4. (As can be seen from Fig. 3.5 later in this chapter, there is rapid degradation when the roll off factor become smaller than 0.4.) The reason for the rapidly degraded performance with smaller excess bandwidth is because of the increased self-noise and due to the fact that the transition region shrinks which leads to a very small gain of the detector, making the synchronizer vulnerable to perturbations [12].

The functional diagram of the Gardner's symbol synchronization is shown in Fig. 3.2. This feedback digital timing recovery system consists four blocks: interpolator, TED, loop filter, and controller. The TED uses Gardner algorithm given in (3.9) to calculate the timing error $e(k)$. The error signal $e(k)$ is filtered by a loop filter to be robust to perturbation. Based on the output of the loop filter, the controller block generates μ_k which is proportional to error signal $e(k)$. The interpolator adjusts interpolation filter $h_I(t)$ using μ_k and obtains the correct sample instances. Each functional module in Fig. 3.2 is discussed next.

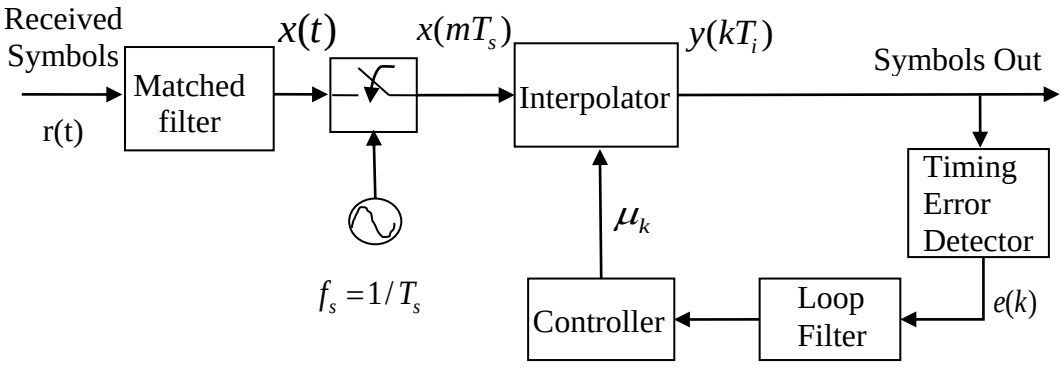

Figure 3.2 Digital timing recovery block diagram.

3.2.1 Interpolator

Assume a baseband signal $x(t)$ is sampled at the sampling frequency $1/T_s$ without aliasing.

$$x(mT_s) = x(m) \tag{3.10}$$

The first step is to put these samples through the interpolator to generate new samples synchronized with symbol rate ($1/T_i$). The interpolator uses a polynomial based interpolation filter $h_I(t)$, which is FIR filter and has $I = I_2 - I_1 + 1$ taps, where I is the length of FIR filter, I1 and I2 are the first and last filter indices, respectively. The time-continuous output of the interpolator can be expressed as

$$y(t) = \sum_m x(mT_s) h_I(t - mT_s) \tag{3.11-a}$$

Resample $y(t)$ at time instant T_i, we get

$$y(kT_i) = \sum_m x(mT_s) h_I(kT_i - mT_s) \tag{3.11-b}$$

where $x(mT_s)$ and $y(kT_i)$ is input and output samples of the interpolator. Generally speaking, T_i / T_s is irrational.

Defined a filter index $i = \text{int}[kT_i / T_s] - m$, basepoint index $m_k = \text{int}[kT_i / T_s]$, and fractional interval part $\mu_k = kT_i / T_s - m_k$, so we have

$$m = m_k - i \tag{3.12-a}$$

$$kT_i - mT_s = (\mu_k + i)T_s \tag{3.12-b}$$

The output of interpolator can be rewritten as

$$y(kT_i) = y[(m_k + \mu_k)T_s] = \sum_{i=I_1}^{I_2} x((m_k - i)T_s)h_I((i + \mu_k)T_s)\,. \tag{3.13}$$

From (3.13), the correct samples can be calculated by I adjacent input samples, and I samples of the impulse response $h_I(t)$. Once having the values m_k and μ_k, and the filter coefficients, the new correct samples are obtained.

There are many kinds of polynomial based interpolation filters, for example linear interpolator, cubic interpolator, and piecewise parabolic interpolator. These filter coefficients $b_l(i)$ can be found in [13]. And the parameter m_k and μ_k are provided by controller section. In this thesis, the piecewise parabolic interpolator is chosen, whose coefficients are given as

$$h_I(t) = \sum_{l=0}^{2} b_l(i)\mu_k^l \tag{3.14}$$

In this case, the output of the interpolator can be expressed as

$$y(k) = \sum_{l=0}^{2} \mu_k^l \sum_{i=I_1}^{I_2} b_l(i)x(m_k - i) \tag{3.15}$$

3.2.2 Timing Error Detector

The timing error detector calculates the error by applying the Gardner algorithm. It checks the difference between three interpolation values at each time instance. Fig. 3.3 shows how to use Gardner algorithm doing timing error computation. According to the (3.8), if we get the correct sampling moment, the error value is zero as shown in Fig 3.3 (a). Otherwise, the error is negative (positive) when the sampling moment is early (late) as shown in Fig. 3.3-b (Fig. 3.3-c).

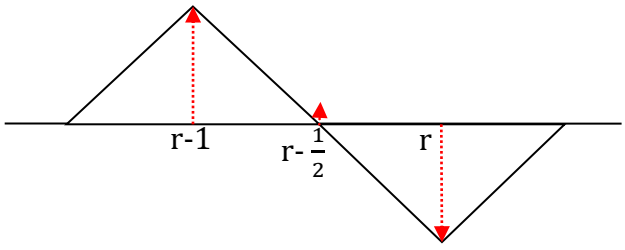

(a)

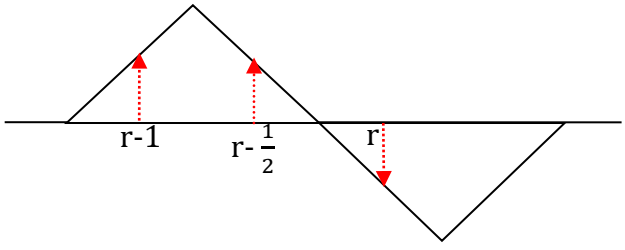

(b)

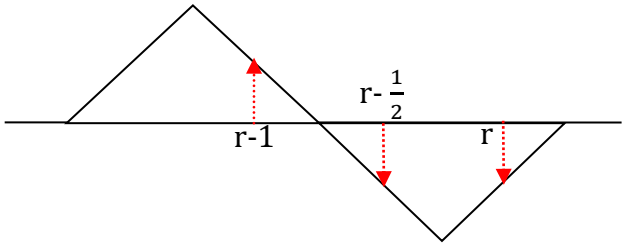

(c)

Figure 3.3 Loop filter block diagram. (a) Correct sampling time. (b) Early sampling time. (c) Late sampling time.

3.2.3 Loop Filter

The effect of the loop filter is to smooth the output errors. It can be seen as a lowpass filter to remove any unwanted high frequency spectral components of the output of the TED.

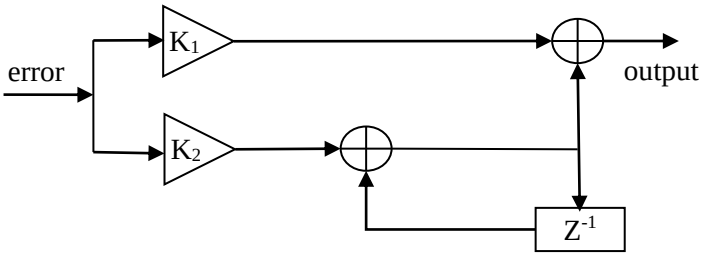

Figure 3.3 Loop filter block diagram.

The parameter K_1 and K_2 in Figure 3.3 are proportional gain and integrator gain, respectively. They can be calculated using (3.16-a), (3.16-b) and (3.16-c), where N is samples per symbol, ξ is damping factor, B_nT_s is normalized loop bandwidth, and K_p is detector gain. Choosing proper values for the parameters are necessary in order to achieve good synchronization performance [15].

$$K_1 = \frac{-4\xi\theta}{(1+2\xi\theta+\theta^2)K_p} \tag{3.16-a}$$

$$K_2 = \frac{-4\theta^2}{(1+2\xi\theta+\theta^2)K_p} \tag{3.16-b}$$

$$\theta = \frac{B_nT_s / N}{\xi + 0.25/\xi} \tag{3.16-c}$$

It is found that, among these parameters, the normalized loop bandwidth B_nT_s is the most sensitive parameter to the convergence time and the stability after convergence. Generally speaking, a large B_nT_s value will make it converge fast, whereas too large B_nT_s will include too much noise, which degrades the accuracy of the synchronization. On the other hand, a small B_nT_s will have more accuracy results. But it takes a long time to converge, requiring lots of training symbols. In many cases, the normalized loop bandwidth is selected based on the minimum input error (TED error) and the noise generated by PLL itself [16].

3.2.4 NCO

The controller provides the interpolator with information m_k and μ_k needed in (3.13). It can be implemented by using a number-controlled oscillator (NCO). The NCO is synchronized with a rate $1/T_s$, and its average output period is T_i. Index m_k is signed at the correct set of signal samples. The fractional part μ_k can be expressed as

$$\mu_k = \frac{\eta(m_k)}{W(m_k)}. \tag{3.17}$$

Here $W(m_k)$ is the control words adjusted by the output of the loop filter, and $\eta(m_k)$ is computed at the *m*-th clock tick.

$$W(m_k) \approx T_s / T_i. \tag{3.18}$$

$$\eta(m) = [\eta(m-1) - W(m-1)] \bmod 1 \tag{3.19}$$

3.3 Simulations

The performance of the Gardner's symbol synchronization method is evaluated in this section for SISO and MIMO systems, respectively.

3.3.1 SISO

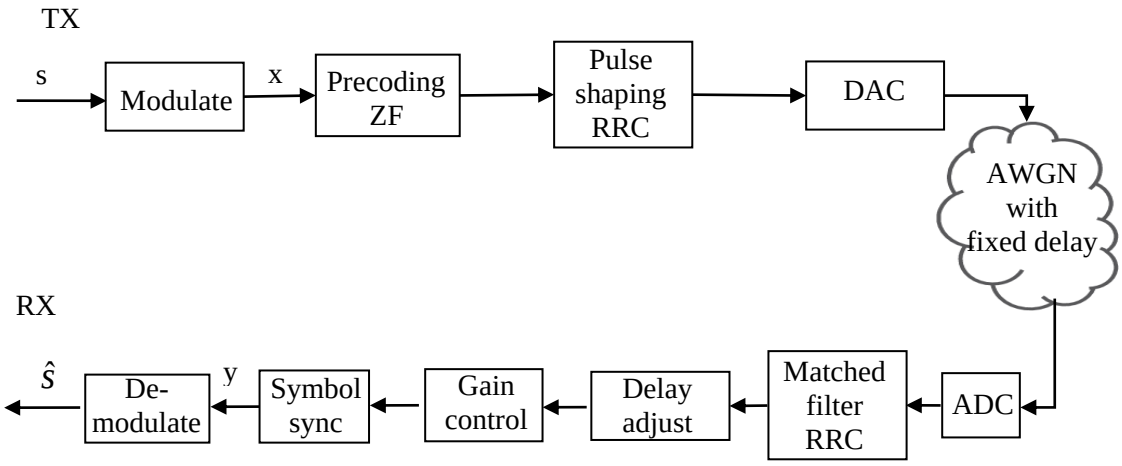

Figure 3.4 Symbol synchronization simulation block diagram for SISO case.

Fig. 3.4 illustrates the model of the symbol synchronization for the SISO case, which is a simplification of the MIMO model shown in Fig. 2.1. In this model, the system chooses RRC pulse for pulse shaping. Note that ZF precoding (of the MIMO case) now simply perform channel inversion (for the SISO case). We add a fixed delay in the channel and AWGN. At the receiver side, we use Gardner's method for symbol synchronization. In order to evaluate the performance of the Gardner's algorithm, we calculate the error vector magnitude (EVM) between received and transmitted signal constellations. EVM is defined as the ratio of the power of the error vector to the root mean square power of the reference (in this case, the reference is the transmitted signal), which is shown as

$$EVM(dB) = 10\log_{10}(\frac{P_{error}}{P_{reference}}) \tag{3.20}$$

With an oversampling factor of four, we find that $B_n T_s$ = 0.0025 is a good compromise between convergence rate and the stability after convergence, as shown in Fig. 3.5 (c). Here, we are interested in the EVM and performance of the symbol synchronization under different roll-off factors, and the corresponding converge performances. We set SNR is 30 dB. The simulation results are shown in Fig. 3.5.

It can be seen from Fig. 3.5 (a), a larger roll-off factor results in a lower EVM (and consequently better performance) at the cost of increased bandwidth. And the roll-off factor should be set higher than 0.4 to ensure the Gardner's algorithm works normally. In Fig. 3.5 (b), after remove the first 150 symbols, the EVM values do not change much. This means that 150 symbols are enough for the system to reach convergence. Moreover, with larger roll off factor, the system converges faster.

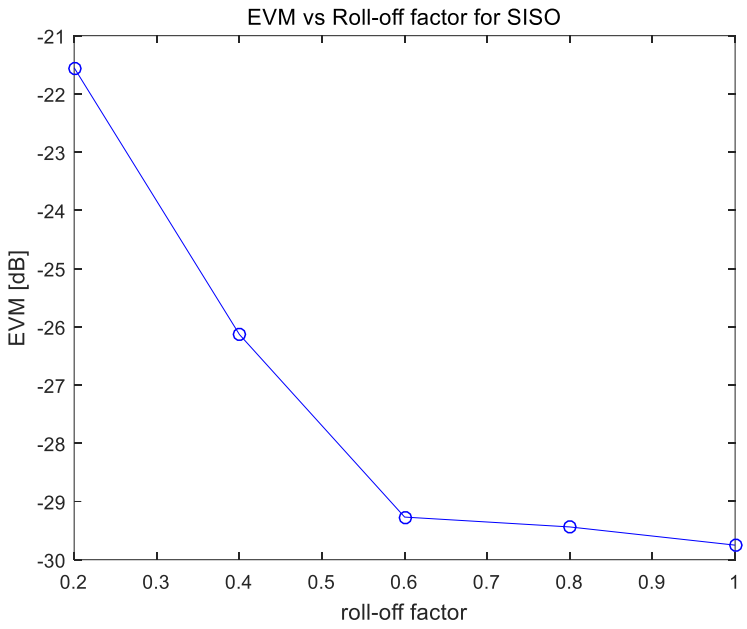
EVM vs Roll-off factor for SISO
EVM [dB]
-21
-22
-23
-24
-25
-26
-27
-28
-29
-30
0.2
0.3
0.4
0.5
0.6
0.7
0.8
0.9
1
roll-off factor

(a)

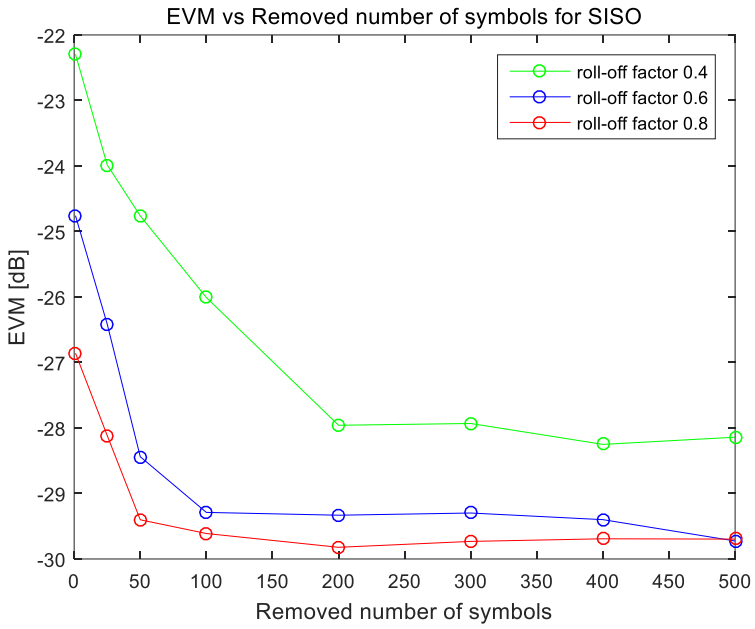
EVM vs Removed number of symbols for SISO
roll-off factor 0.4
roll-off factor 0.6
roll-off factor 0.8
EVM [dB]
-22
-23
-24
-25
-26
-27
-28
-29
-30
0
50
100
150
200
250
300
350
400
450
500
Removed number of symbols

(b)

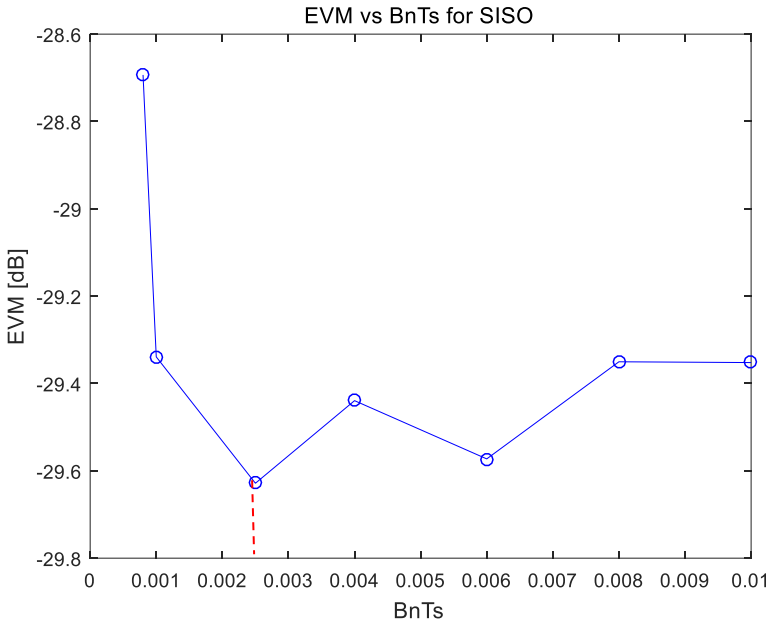

(c)

Figure 3.5 EVM with different Roll-off factors for the SISO case. (a)EVM as a function of Roll-off factor for the SISO case by removing the first 150 symbols. (b) EVM calculated by removing different number of symbols under different roll-off factors. (c)EVM (by removing the first 150 symbols) as a function of BnTs factor for the SISO case with oversampling factor of 4, roll-off factor of 1.

3.3.2 MIMO

In SISO system, there is only a single timing offset needs to be estimated. While in (multi-user) MIMO system, each user has its own independent clock and each transmit-receive antenna pair may experience slightly different delays. (In the simulation, each BS antenna is assigned to a distinct delay.) These cause multiple timing offsets between transmitter and receiver [17].

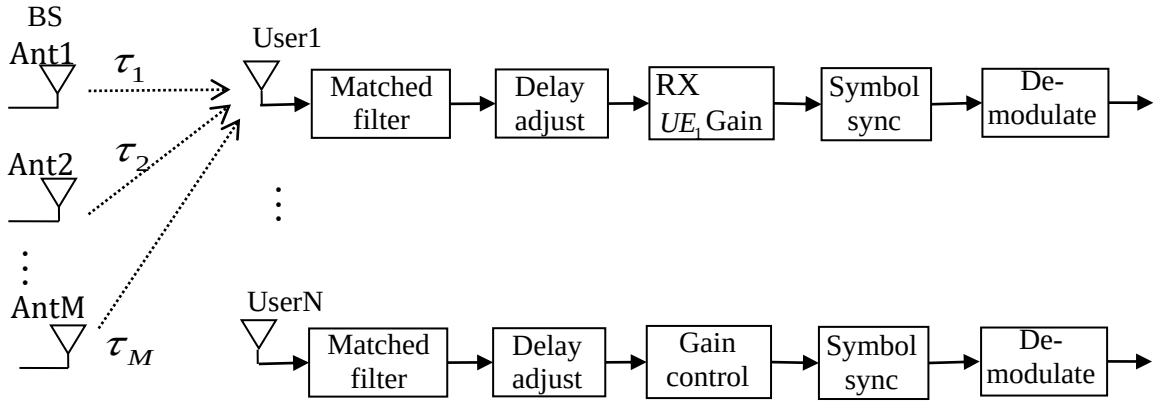

Figure 3.6 Symbol synchronization block diagram for MIMO case.

Fig. 3.6 shows the considered transceiver architecture. We implement symbol synchronization for each user separately. Assume the system has N users and M base station antennas. In the downlink, M antennas transmit symbols to each user, e.g. transmitting $a_i(k)$ to the i-th user ($i = 1, 2 \cdots N$). We add fixed time delay for each path, e.g., $\tau_{m,i}$ is the fixed delay in the path from m-th base station antenna to i-th user. Therefore, each user is confronted with M different fixed delays. For user i, the received signal can be expressed as

$$r_i(t) = \sum_{m=1}^{M} \sum_{k=0}^{K-1} a_i(k) v(t - kT - \tau_{m,i}) + \omega_i(t) \qquad i = 1 \cdots N \tag{3.21}$$

where K is frame length for each user, $v(t)$ is the transmitter pulse filter that is assumed to be the same for all the users, and $\omega_i(t)$ is the AWGN at the i-th user.

The symbol synchronization method used in the MIMO case is a straightforward extension of the Gardner's algorithm of the SISO case. Each user applies the Gardner's algorithm on its own received signal (3.21).

The symbol synchronization simulation results for the multi-user MIMO case is shown in Fig. 3.7. Note that the slight EVM variation is due to different realization of noise. Increasing the number of users or BS antennas almost does not affect the performance of the symbol synchronization. So it is safe to conclude that the Gardner's method can be readily applied to the downlink massive MIMO scenario.

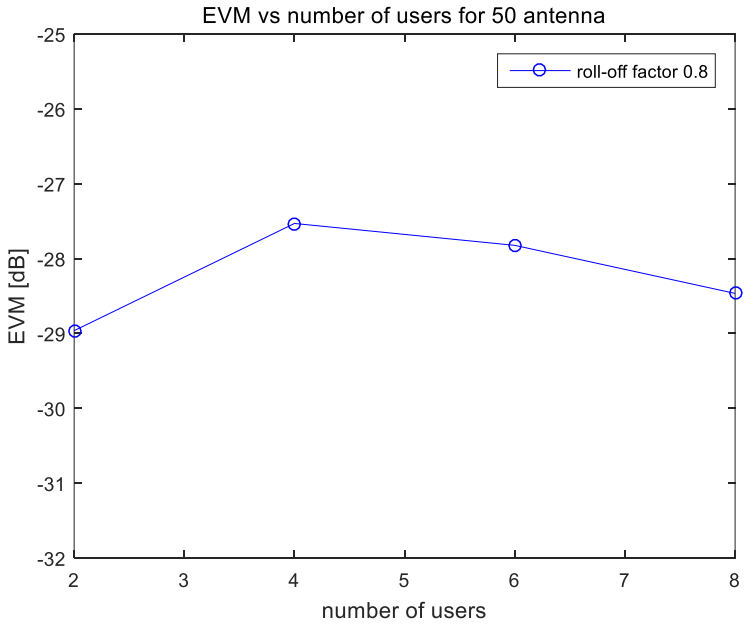

(a)

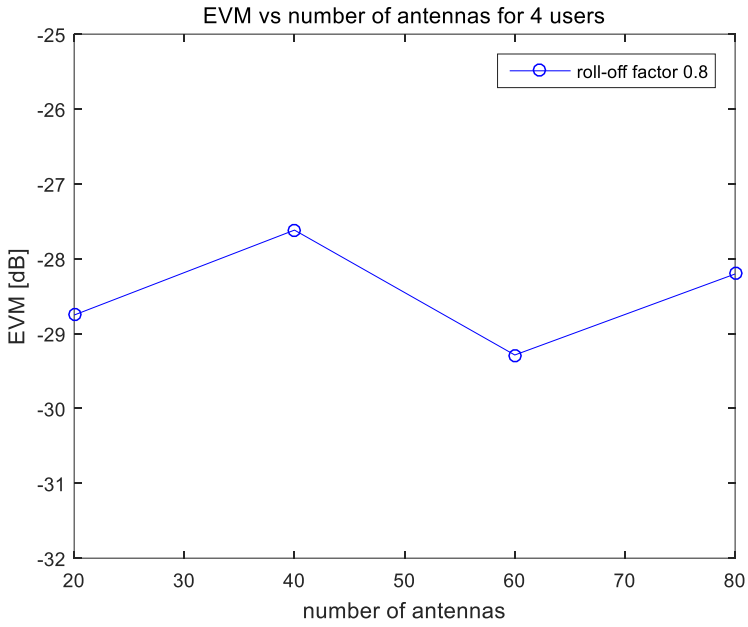

(b)

Figure 3.7 EVM with Roll-off factor 0.8 and 30-dB SNR for the MIMO case. (a) EVM for different numbers of users and 50 BS antennas. (b) EVM for different numbers of BS antennas and 4 users.

4 Channel Estimation

Multipath fading channels for broadband communication are usually frequency selective. Channel estimations make it possible to adapt transmissions to channel conditions in order to achieve acceptable performance in multipath fading environments. For instance, implementing equalization to avoid ISI requires CSI. In massive MIMO system, channel estimation is crucial for downlink precoding. Without reliable CSI estimation, the performance of the massive MIMO system will degrade. In this section, we assume the OFDM technique is used in combination of the MIMO system, i.e., MIMO-OFDM system.

4.1 Multipath Fading Channel

In multipath fading channel, due to the mobility of the user and the scattering of the propagation environment, many signal paths exist and this path can add up constructively or destructively. As a result, the channel changes randomly with time and frequency. Compared with transmitted signal bandwidth and symbol duration, wireless channel is roughly divided into four types: flat fading, frequency selective fading, fast fading, and slow fading [18]. For high data rate streams, since the transmitted signals occupy wide bandwidths, the multipath channels are usually frequency selective channel (provided that the coherence bandwidth of the channel is comparable or smaller than the transmitted signal bandwidth). A time-varying and frequency-selective channel can be modeled in Fig. 4.1 [18], where T_s sampling interval, $c_l(t)$ and τ_l are the channel impulse response of the l-th channel tap, respectively, and there are in total L channel taps.

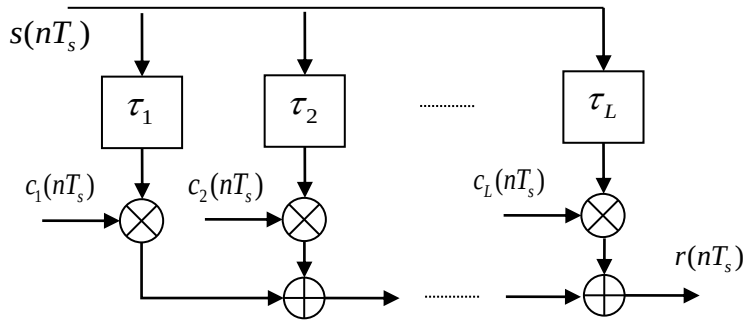

Figure 4.1 Discrete-time model of a time and frequency-varying channel.

The received signal, passing through the multipath channel, can be expressed as

$$r(nT_s) = \sum_{l=1}^{L} c_l(nT_s)s(nT_s - \tau_l T_s) \tag{4.1}$$

And the channel frequency response is given as

$$C(f, nT_s) = \sum_{l=1}^{L} c_l(nT_s) \exp(-j2\pi f \tau_l T_s) \tag{4.2}$$

4.2 OFDM

The OFDM is widely used in wireless communication systems for its attractive properties. It divides the bandwidth into multiple orthogonal narrowband sub-channels. In this way, a frequency selective channel is converted into multiple flat fading channels, which significantly simplifies the channel equalization. Combine OFDM with MIMO is a popular technique. Since MIMO technique increases channel capacity significantly in a flat fading channel, along with OFDM which could convert frequency selective channel into flat sub-channels, MIMO-OFDM system can achieve high data rates with one-tap equalizer [19].

In this thesis, we first discuss the OFDM system for the SISO case, where an OFDM symbol with N subcarriers can be written as

$$x(n) = \sum_{k=0}^{N-1} s(k) e^{j2\pi kn/N} \qquad n = 0,1 \cdots N-1 \tag{4.3}$$

where $s(k)$ is the symbol on the k-th subcarrier and x is the time-domain OFDM signal. Usually, N is chosen to be a power of 2 (with possible zero padding) so that the (inverse) discrete Fourier transform can be implemented conveniently via (IFFT) FFT.

Transmitting OFDM symbols through the multipath channel h, the received signal can be expressed as

$$y(n) = x(n) * h(n) + \omega(n) \tag{4.4}$$

where * denotes convolution. Because the channel has time-dispersion, two adjacent OFDM symbols may have ISI. Since the channel usually has finite length, the received signal will be stationary after the length of channel. The ISI is usually avoided by adding a cyclic prefix (CP) to the time-domain OFDM symbol before transmission. The CP should be larger than the channel length in order to eliminate the ISI between OFDM symbols, yet it should not be unnecessarily long for it is an overhead for the communication system [20].

At the receiver, after CP removal, the frequency domain OFDM signal can be expressed as

$$Y(k) = H(k)X(k) + W(k) \tag{4.5}$$

where H is the channel frequency response, and X, Y and W are the transmitted signal , received signal and AWGN in the frequency-domain, respectively.

4.3 LS Channel Estimation

Channel estimation techniques can be divided into two categories: data aided (using training symbols) and non-data aided (blind channel estimation). For OFDM systems, the non-data aided method usually makes use of the presence of CP or finite alphabet property of the input data. Since it does not require any preamble, the non-data aided channel estimation enjoys high spectrum efficiency. However, it usually requires many signal samples before reaching convergence, which results in long estimation latency. The data-aided channel estimation, on the other hand, is widely used because of its reliable estimation performance. There are many data-aided channel estimation techniques, for example: least square (LS), minimum mean-square error (MMSE), and maximum likelihood (ML) algorithms. Here we use LS algorithm for it simple implement [21].

4.3.1 SISO

For SISO-OFDM system, sending a pilot X_p through the channel and neglecting the subcarrier index, the received signal can be expressed similar to (4.5)

$$Y_p = X_p H + W_p \tag{4.6}$$

The LS channel estimation is to find $\hat{H}$ that minimize the mean square error or the channel estimate

$$\hat{H} = \arg\min_{H} \left\| Y_p - X_p H \right\|^2 \tag{4.7}$$

which is equivalent to find $\hat{H}$ satisfying

$$\frac{\partial \left\{ (Y_p - X_p H)^* (Y_p - X_p H) \right\}}{\partial \hat{H}} = 0 \tag{4.8}$$

The LS channel estimate is

$$\hat{H}_p = (X_p^H X_p)^{-1} X_p^H Y_p = X_p^+ Y_p \tag{4.9}$$

We will extend the LS channel estimation to the MIMO-OFDM system next.

4.3.2 MIMO

For the MIMO case, we use the same idea as the SISO case, but the implementation is slightly more complicated. Since in a massive MIMO system, the number of BS antennas can be much larger than the number of users, doing channel estimation in the DL consumes much more pilots than that in the UL [1]. For this reason, it is usually assumed that the massive MIMO system will use TDD. In a TDD-based massive MIMO system, the channel estimation can be done in the UL at the BS, which then use the estimated channel for precoding in the DL.

In order to illustrate the channel estimation in MIMO-OFDM system clearly, we first consider a simple example. Assume there are three base station antennas and two users, as shown in Figure 4.2.

The *l*-th tap of the MIMO channel impulse response is a 3×2 matrix $\tilde{\mathbf{H}}_l$

$$\tilde{\mathbf{H}}_l = \begin{bmatrix} h_{11,l}\, h_{12,l} \\ h_{21,l}\, h_{22,l} \\ h_{31,l}\, h_{32,l} \end{bmatrix} \tag{4.10}$$

While the channel input-output relation can be expressed as

$$\mathbf{r}(n) = \sum_{l=0}^{L-1} \tilde{\mathbf{H}}_l \mathbf{x}(n-l) + \boldsymbol{\omega}(n) \tag{4.11}$$

In frequency domain, the input-output relation becomes

$$\mathbf{y}(k) = \mathbf{H}(k)\mathbf{s}(k) + \mathbf{w}(k) \tag{4.12}$$

where $\mathbf{H}(k)$ is 3×2 matrix containing the channel frequency response at the *k*-th subcarrier. The task is to estimate the channel matrix $\mathbf{H}$ at each of the subcarriers. Note that, for notational convenience, the subcarrier index has been omitted in the following expressions.

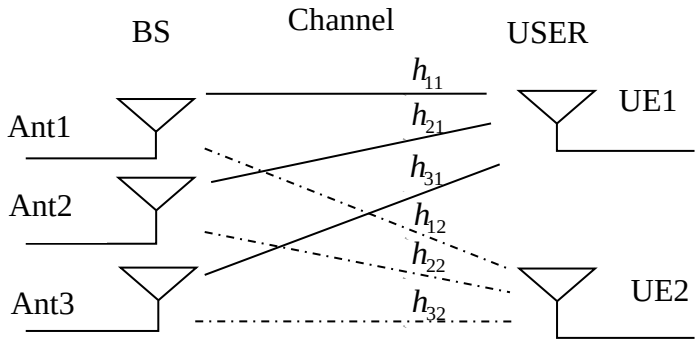

Figure 4.2 MIMO system with three BS antennas and two users.

In OFDM system, channel is flat in each subcarrier, provided that there are large enough subcarriers. According to Fig. 4.3, at each subcarrier, there are 6 unknowns which need 6 equations. This means that, in the transmitter side, two OFDM symbols need to be send from each user, e.g. $user_1$ sends OFDM symbol a_1 in first time slot and a_2 in second time slot, so does $user_2$. In order to make sure that the two users do not interference each other, the OFDM pilots send by each user should be orthogonal with other users. That is, a_1 and a_2 need to be orthogonal with b_1 and b_2. Ignoring the noise for now, we get six equations from the three receiving antenna at two time slots, which is enough to solve the six unknown CSI.

$$y_{11} = H_{11}a_1 + H_{12}b_1 \quad (4.13\text{-a})$$
$$y_{21} = H_{21}a_1 + H_{22}b_1 \quad (4.13\text{-b})$$
$$y_{31} = H_{31}a_1 + H_{32}b_1 \quad (4.13\text{-c})$$
$$y_{12} = H_{11}a_2 + H_{12}b_2 \quad (4.13\text{-d})$$
$$y_{22} = H_{21}a_2 + H_{22}b_2 \quad (4.13\text{-e})$$
$$y_{32} = H_{31}a_2 + H_{32}b_2 \quad (4.13\text{-f})$$

Using the LS algorithm, we have the channel estimate as

$$\hat{\mathbf{H}} = \mathbf{Y}\mathbf{X}^{+} = \mathbf{Y}\mathbf{X}^{H}\left(\mathbf{X}\mathbf{X}^{H}\right)^{-1} \quad (4.14)$$

where the superscript $^{+}$ denotes pseudo-inverse, $\mathbf{X} = \begin{bmatrix} a_1 & a_2 \\ b_1 & b_2 \end{bmatrix}$, $\mathbf{Y} = \begin{bmatrix} y_{11} & y_{12} \\ y_{21} & y_{22} \\ y_{31} & y_{32} \end{bmatrix}$ and $\hat{\mathbf{H}} = \begin{bmatrix} H_{11} & H_{12} \\ H_{21} & H_{22} \\ H_{31} & H_{32} \end{bmatrix}$.

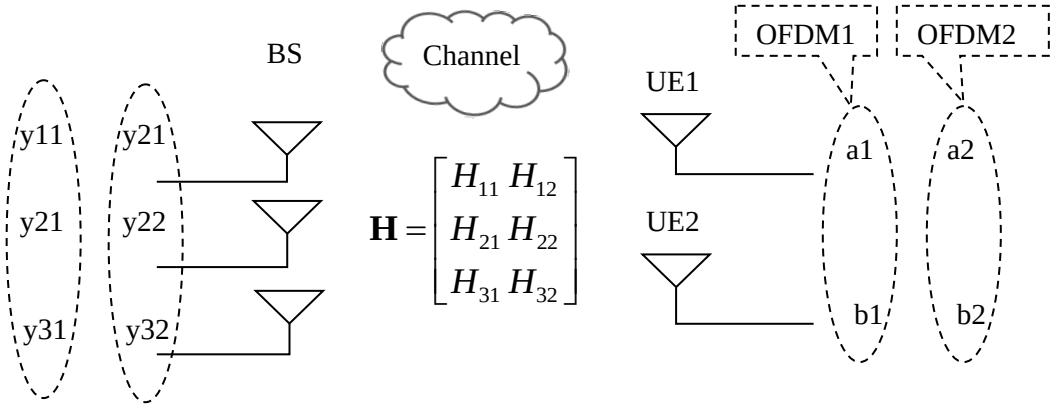

Figure 4.3 Channel estimation in uplink for MIMO-OFDM system.

From **H** in the frequency domain, we get zero forcing precoding matrix **G** for each subcarrier

$$\mathbf{G}=\mathbf{H}^{+} \quad (4.15)$$

The extension of the LS channel estimation method to the general massive MIMO case is straightforward. In principle, each user needs to transmit (at least) K training (orthogonal) OFDM symbols, where K is the number of users. The training signals **X** in (4.14) is a $K \times K$ matrix, while the received signal **Y** is a $M \times K$ matrix with M denoting the BS antenna number.

4.4 Simulations

In this section, we evaluate the performance of the LS channel estimation via simulations. A frequency-selective channel with four channel taps, each with Rayleigh fading, is assumed in generating the multipath channel. The OFDM has 64 subcarriers and a CP length of 6 samples.

First, we check the performance of estimated channel frequency response both in SISO and MIMO case. Since the channel estimate is used for equalization, the channel estimation error will be directly reflected in the EVM performance of the system. Therefore, we will evaluate the channel estimation performance in terms of EVM between the transmitted and received signal. Specifically, we first estimate the channel in the presence of AWGN and multipath channel in the UL. Then, we apply channel inversion using the estimated channel with the same multipath channel yet in the absence of AWGN in the DL. In this way, the EVM is only caused by the channel estimation error.

4.4.1 Performance of Channel Estimation

We first shows the estimated Rayleigh fading channel frequency response without AWGN for SISO, then compare the mean square error (MSE) between estimated channel frequency response and the original channel both for SISO and MIMO case with AWGN.

4.4.1.1 SISO

Fig. 4.4 shows the magnitude and phase of the estimated channel frequency response in the absence of AWGN together with the true values.

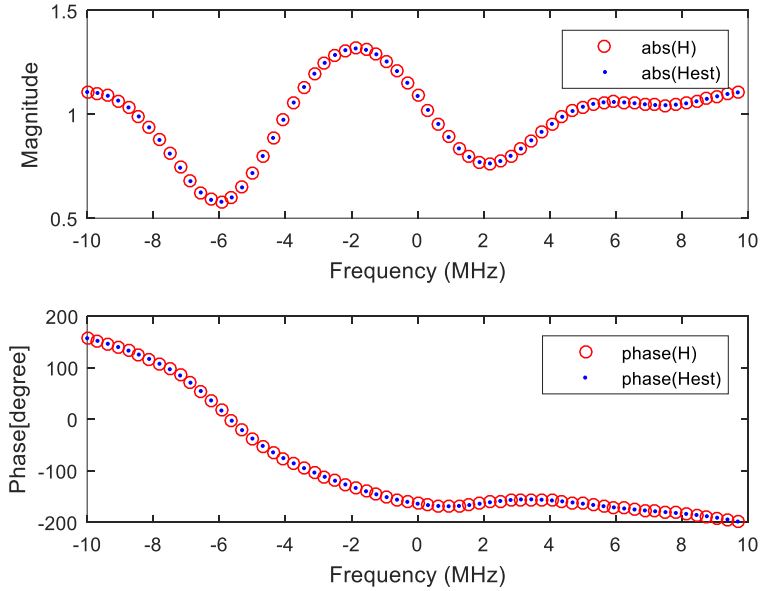

Figure 4.4 Estimated channel frequency response without AWGN.

Fig. 4.5 shows the MSE of the channel estimation (calculated using 100 OFDM symbol pilots) as a function of SNR.

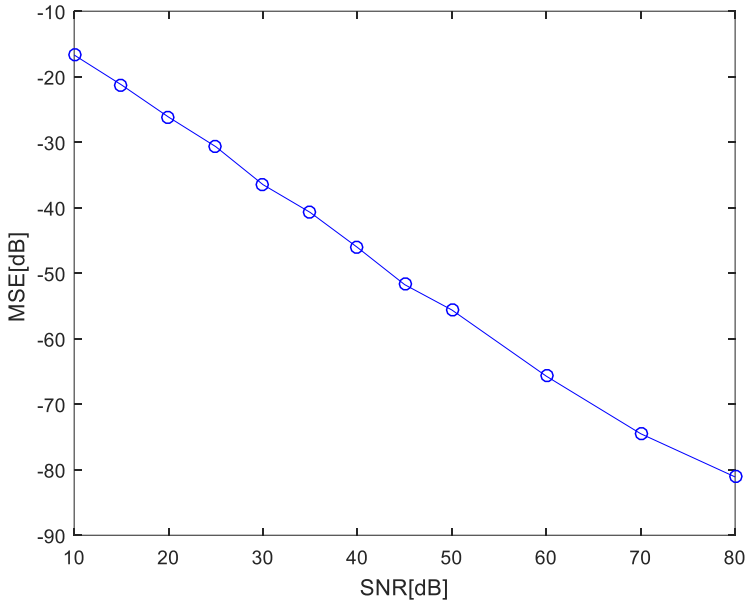

Figure 4.5 MSE of the estimated channel.

4.4.1.2 MIMO

Fig. 4.6 shows the MSE of the channel estimation (calculated using 100 MIMO-OFDM symbol pilots) for four base station antennas and four users.

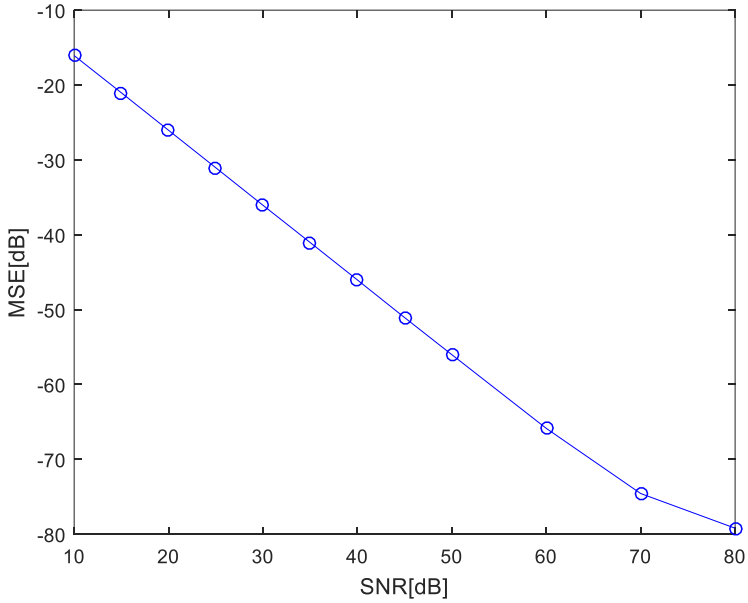

Figure 4.6 MSE of the estimated channel for four base station antennas and four users.

Note that by increasing the BS antennas to 100, the channel estimation performance is about the same.

4.4.2 Equalization performance

In the UL, the channel is estimated in the presence of AWGN and multipath channel. The estimated channel is used for DL ZF precoding in the absence of AWGN. The Gram-Schmidt procedure is used to generating orthogonal pilots that are necessary for MIMO channel estimation, see (4.14).

Fig. 4.7 shows the DL EVM when the estimated channel in UL is used for DL ZF precoding. In Fig. 4.7 (a), the EVM decreases as the number of BS antennas increases. That is true since more BS antennas (with fixed user number) will have larger diversity order [10]. In the same way, if we fixed the BS antennas, the less user number has more accurate channel estimation, see Fig. 4.7 (b).

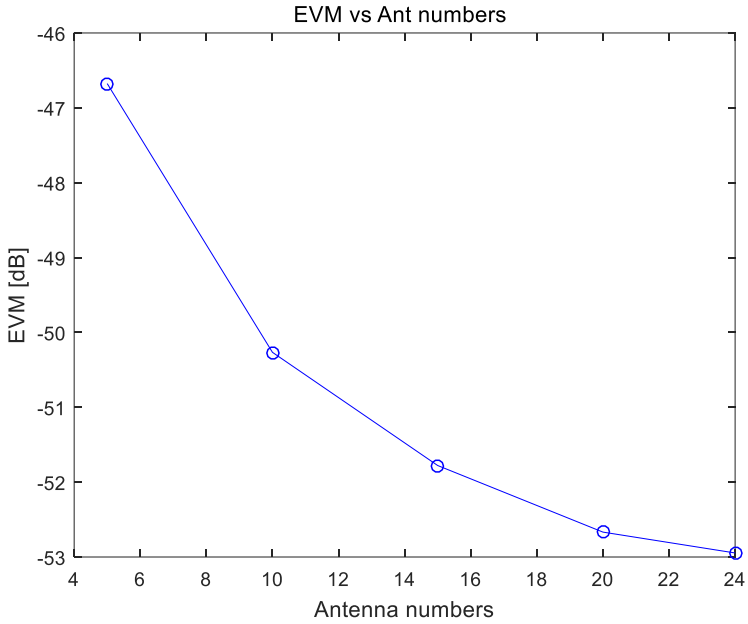

(a)

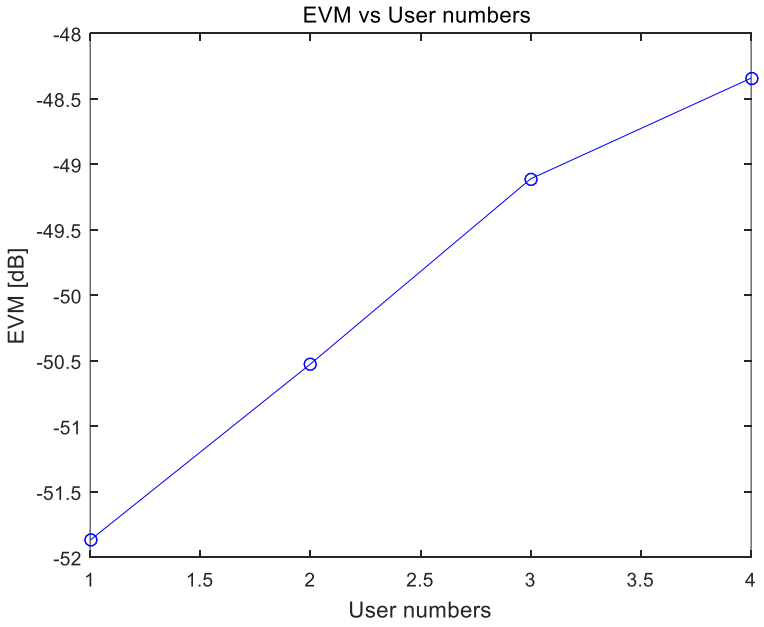

(b)

Figure 4.7 EVM for the Massive MIMO DL. The SNR is for the UL where the channel estimation is performed. (a) EVM as a function of the number of BS antennas for 2 user and 30-dB UL-SNR. (b) EVM as a function of the number of users for 10 BS antennas 30-dB UL-SNR.

5 Frequency Synchronization

It is well known that the OFDM system is robust to the delay spread of the multipath channel. However, OFDM systems are sensitive to the CFO, which will destroy the orthogonality of the subcarriers and degrade the system performance severely. The CFO caused by the mismatch between local oscillator of the transmitter and that of the receiver [22]. Multi-user MIMO-OFDM systems are even more sensitive to CFO, since each user has an independent oscillator and, therefore, a distinct CFO, making the (direct) UL frequency synchronization a challenging task [23].

In this chapter, we deal with the CFO for OFDM systems. We first present the symbol synchronization for SISO system and then extend it to the massive MIMO system.

5.1 CFO Estimation

In the literature, many schemes have been proposed to estimate the CFO. They are divided, in general, into two categories: data-aided method (using dedicated synchronization pilots) and blind estimation method (without using pilots). The data-aided method has better performance at the cost of reduced spectral efficiency [22]. Since the OFDM system is sensitive to CFO, the data aided method is chosen in this thesis.

Fig. 5.1 illustrate the generation of the CFO, which is due to the mismatch Δf between the oscillators at the transmitter and the receiver.

Figure 5.1 The generation of carrier frequency offset.

The CFO causes a linear phase rotation of the time-domain signal, see (5.1). Hence, the typical data-aided method for CFO estimation is to measure this phase rotation. Note that the CFO estimator is derived under the AWGN channel assumption [24]. The received signal can be written as

$$y(n) = x(n)e^{j2\pi\Delta f n T_S} + \omega(n) \tag{5.1}$$

For expression convenience, in this thesis, we use the normalized CFO, define as

$$\varepsilon = \frac{\Delta f}{f_s} \tag{5.2}$$

where f_s is sampling frequency. So (5.1) can be rewritten as

$$y(n) = x(n)e^{j2\pi\Delta f n T_S} + \omega(n) = x(n)e^{j2\pi\varepsilon n} + \omega(n) \tag{5.3}$$

Now the task is to estimate ε. Divide both sides of (5.3) by $x(n)$ and define the function as $f(n)$

$$f(n) = \frac{y(n)}{x(n)} = e^{j2\pi\varepsilon n} + \frac{\omega(n)}{x(n)} \tag{5.4}$$

After Δn time samples, (5.4) can be written as

$$f(n+\Delta n) = e^{j2\pi\varepsilon n + j2\pi\varepsilon\Delta n} + \frac{\omega(n+\Delta n)}{x(n+\Delta n)} \tag{5.5}$$

The normalized CFO ε in (5.4) and (5.5) are identical. Now define a new function σ as [24]

$$\begin{aligned} \sigma &= \sum_{n=1}^{N-\Delta n} f(n) f^*(n+\Delta n) \\ &\approx \sum_{n=1}^{N-\Delta n} e^{-j2\pi\Delta n} \\ &= (N-\Delta n) e^{-j2\pi\varepsilon\Delta n} \end{aligned} \tag{5.6}$$

The approximation in (5.6) holds because $\omega(n)$, $\omega(n+\Delta n)$, and the CFO term $e^{j2\pi\varepsilon n}$ are uncorrelated.

The normalized CFO can then be estimated as

$$\varepsilon = \frac{\angle(\sigma)}{-2\pi\Delta n} = \frac{\angle\left(\sum_{n=1}^{N-\Delta n} f(n) f^*(n+\Delta n)\right)}{-2\pi\Delta n} \tag{5.7}$$

where the function $\angle(\bullet)$ takes the phase angle of its argument. The CFO estimation range is related to f_s and Δn [24]

$$|\Delta f| \le \frac{f_s}{2\Delta n} \tag{5.8}$$

From (5.8), the estimation range can be increased by reducing the sample step Δn. Once the CFO is estimated, it can be compensated easily by multiply the received signal by $e^{-j2\pi\Delta f n T_S}$

$$y(n) \times e^{-j2\pi\Delta f n T_S} = [x(n) e^{j2\pi\Delta f n T_S} + \omega(n)] \times e^{-j2\pi\Delta f n T_S} \tag{5.9}$$

5.2 Simulation

The CFO estimation and compensation is carried out in time domain. To evaluate the estimation performance, the simulation results are shown for SISO and MIMO cases next, respectively, with SNR is 30dB. The sampling frequency is chosen as 20 MHz, subcarrier number N = 64 and sample step of Δn = 4.

5.2.1 SISO

The block diagram for the SISO case is shown in Figure 5.2.

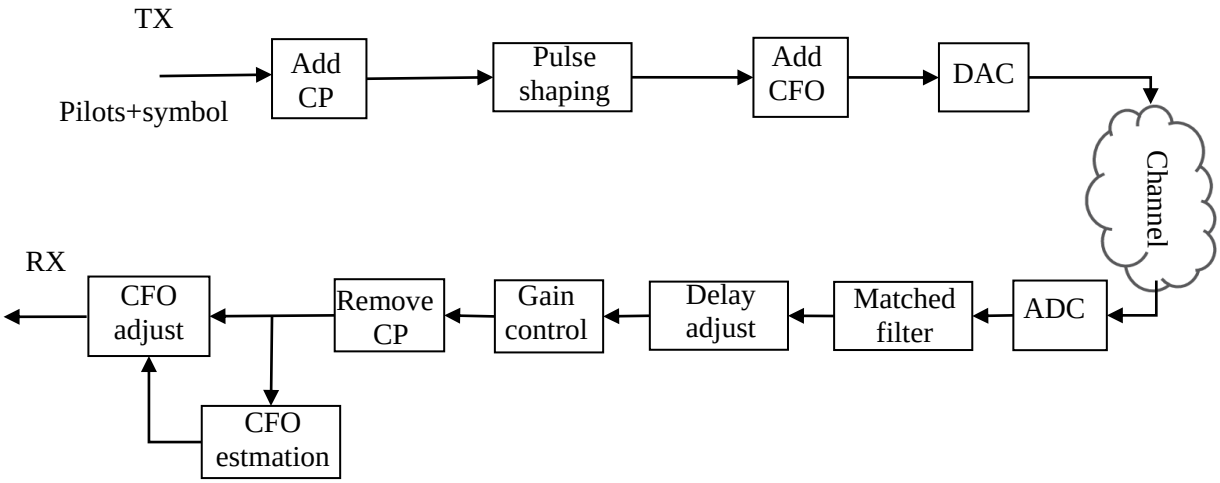

Figure 5.2 CFO estimation and compensation block diagram for SISO.

Fig. 5.3 shows the mean square error (MSE) of the CFO estimation as the CFO increases. As the CFO increases up to 2.5 MHz, the MSE performance degrades drastically. According to the estimation range (5.8) , when f_s = 20 MHz, N = 64, and Δn =4, the maximum absolute value of CFO that can be estimated is 2.5MHz. When CFO under 2.5MHz, the MSE performance keeps the same at different CFO values.

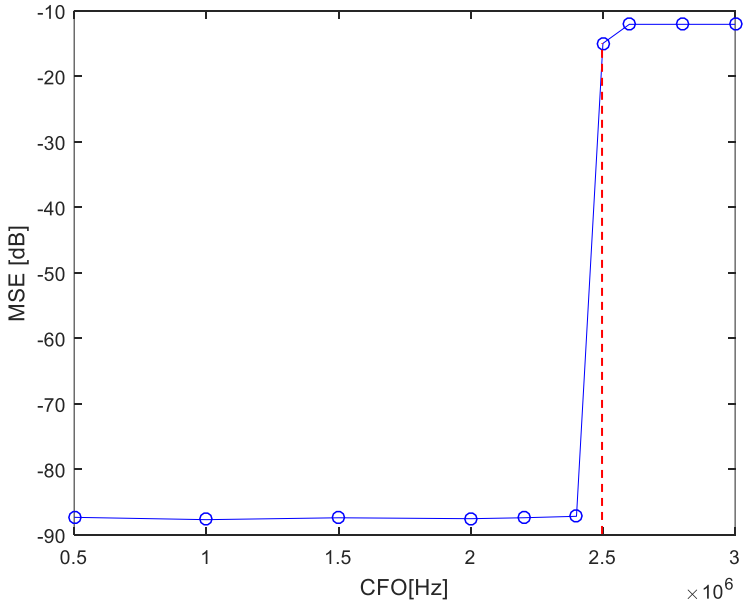

Figure 5.3 MSE of the CFO estimation for the SISO case.

5.2.2 MIMO

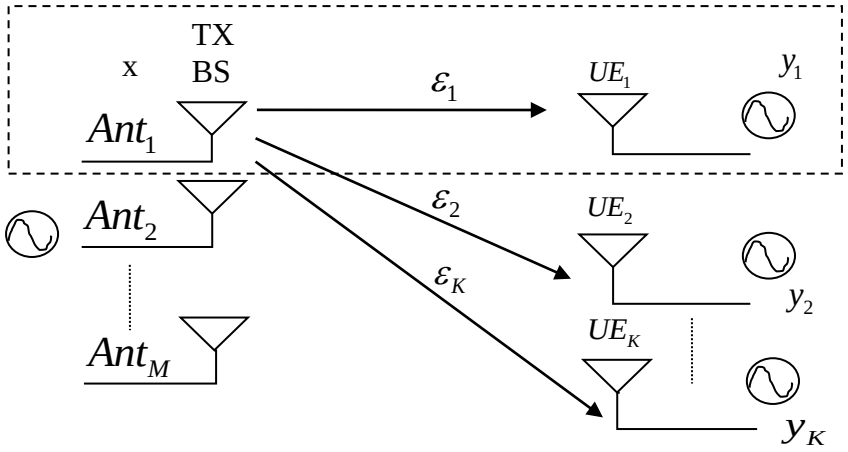

Figure 5.4 CFOs in DL multi-user MIMO-OFDM system.

Unlike the SISO case, in the multi-user MIMO-OFDM system, all the BS antennas share the same local oscillator, while each user has an independent local oscillator. As shown in Fig. 5.4, there are *M* BS antennas and *K* users, each user see a different CFO, which is the difference between the BS oscillator and the user's oscillator. The CFO normalized by the sampling frequency is denoted as $\varepsilon_1, \varepsilon_2, \cdots, \varepsilon_K$.

The joint CFO estimation in the UL multi-user MIMO system is a nontrivial task. One simple way to solve this problem is to estimate the CFO for each of the user in the DL.
We only use one BS antenna sending pilots and symbols to all the users. For example, in Fig. 5.4, we choose Ant_1 in BS to transmit symbols to all the user $UE_1, UE_2 \cdots\cdots UE_k$. In order to solve the UE_1's CFO ε_1, we use the transmitted symbols $x(n)$, and the received symbols $y_1(n)$. According to (5.10) and (5.11) below, we derive the estimated CFO ε_1 for UE_1. In this way, each user estimates its own CFO using the same approach as in the SISO case. Then adjust its transmission using the estimated CFO for UL transmission [23].

$$f_i(n) = \frac{y_i(n)}{x(n)} = e^{j2\pi\varepsilon_i n} + \frac{\omega_i(n)}{x(n)} \qquad i = 1 \cdots K \tag{5.10}$$

$$\varepsilon_i = \frac{\angle \sum_{n=1}^{N-\Delta n} f_i(n) f_i^*(n+\Delta n)}{-2\pi\Delta n} \qquad i = 1 \cdots K \tag{5.11}$$

Fig. 5.5 shows the MSE of the CFO estimation as a function of user number for the multi-user MIMO system in the DL. Each user is assigned a random CFO, ranging from 0.16 to 1.6 MHz and SNR is 30dB. As expected, increasing the number of users will not affect the CFO estimation performance, since the DL case is similar to that of the SISO system.

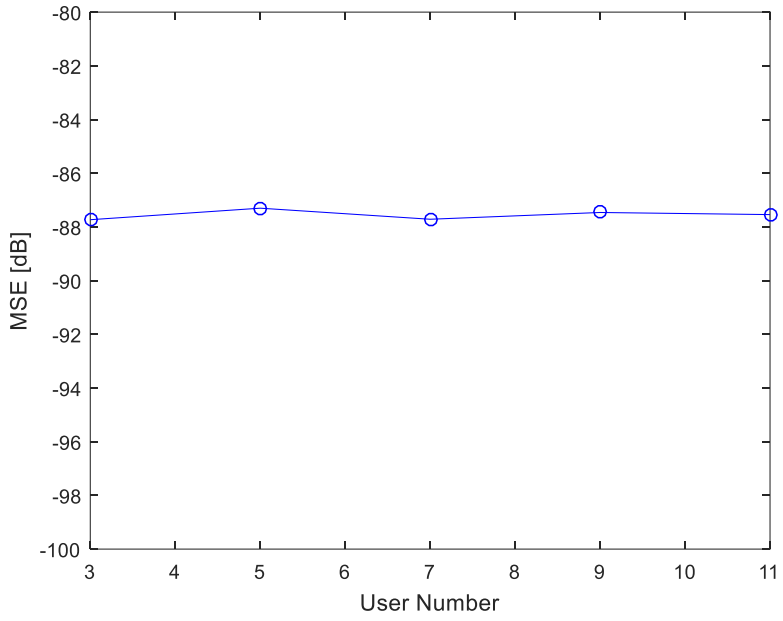

Figure 5.5 MSE of CFO estimation in DL as a function of user number.

6 Conclusion

The massive MIMO system has received lots of attention for its potential of increasing data rate, improving reliability and energy efficiency, and reducing interferences. However, the massive MIMO system, equipped with hundreds of (or even more) BS antennas, also imposes challenges in signal processing complexity and hardware costs. While it is impossible to address all of the challenging issues, this thesis is devoted to studying symbol synchronization, frequency synchronization and channel estimation for the massive MIMO system. The symbol synchronization is studied for the SC-based massive MIMO system. It is found that the popular Gardner's algorithm that has been used for symbol synchronizations in SISO systems can be readily applied for the massive MIMO system. Channel estimation and frequency synchronization are considered for OFDM-based massive MIMO systems. Due to the large number of BS antennas, the pilot-based channel estimation in the DL will cause too much overhead. As a result, the TDD is assumed in this thesis. And we apply the standard least-square channel estimation in the UL, and the estimated channel is then used for MIMO precoding in the downlink (DL). Similarly, the joint estimation of the CFOs of all the users in the UL will drastically increase the complexity of the system. Therefore, it is assumed, in this thesis, that each user estimates its CFO during the DL and adjusts its transmission accordingly in the UL. In this way, the CFO estimation is basically the same as that for the SISO system. All these three topics are studied and verified by extensive simulations in this thesis.

7 References

[1] E. G. Larsson, O. Edfors, F. Tufvesson and T. L. Marzetta, "Massive MIMO for next generation wireless systems," IEEE Communications Magazine, vol. 52, no. 2, pp. 186-195, Feb. 2014.

[2] C. C. Jay Kuo, S. H. Tsai, L. Tadjpour and Y. H. Chang, "Precoding Techniques for Digital Communication Systems," Springer US, pp. 3-10, 2008.

[3] X. Gao, O. Edfors, F. Rusek, and F. Tufvesson, "Linear pre-coding performance in measured very-large MIMO channels," *IEEE VTC Fall*, San Francisco, CA, Sep. 2011, pp. 1-5.

[4] J. B. Anderson, Digital Transmission Engineering, 2nd edition, A John Wiley & Sons, Inc., 2005.

[5] Root-raised-cosine filter. https://en.wikipedia.org/wiki/Root-raised-cosine_filter.

[6] S. Al-Majmaie. *IQ imbalance compensation: blind versus pilot-based algorithms, using different IQ imbalance models*. Master thesis, Lund University, 2014.

[7] M. Reza Khanzadi, *Phase Noise in Communication Systems*, PHD thesis, Chalmers University of Technology ,2015.

[8] M. Benssalah and M. Djeddou, "Implementation of synchronization algorithms, carrier phase recovery and symbol timing recovery on a digital signal processor," *International Symposium on Signals, Circuits and Systems*, Lasi, 9-10 July 2009.

[9] Z. Liu and K. Yi, "Symbol Timing Synchronization Using Interpolation-Based Matched-Filters," *Wireless Pers. Commun.*, vol. 50, pp. 457–467, 2009.

[10] A. Paulraj, R. Nabar and D. Gore, Introduction to Space-time Wireless Communication, Cambridge university press, 2003.

[11] J. Zhang, L. Tian, Y. Wang, and M. Liu, "Selection Transmitting/Maximum Ratio Combiningfor Timing Synchronization of MIMO-OFDM systems," *IEEE Trans. Broadcasting*, vol. 60, no. 4, pp. 626-636, Dec. 2014.

[12] F. M. Gardner, "A BPSK/QPSK Timing-Error Detector for Sampled Receivers," IEEE Trans. Commun., vol. 34, no. 5, pp. 423-429, May 1986.

[13] F. M. Gardner, "Interpolation in Digital Modems-Part I: Fundamentals," *IEEE Trans. Commun.*, vol. 41, no. 3, pp. 501-507, Mar. 1993.

[14] L. Erup, F. M. Gardner, and R. A. Harris “Interpolation in Digital Modems-Part II: Implementation and Performance,” *IEEE Trans. Commun.*, vol. 41, no. 6, pp. 998-1008, Jun. 1993

[15] *Documentation: correct symbol timing clock skew*, MathWorks, 2016

[16] D. Lim, “A Modified Gardner Detector for Symbol Timing Recovery of M-PSK Signals,” *IEEE Trans. Commun.*, vol. 52, no. 10, pp. 1643-1647, Oct. 2004.

[17] A. A. Nasir S. Durrani R. A. Kennedy, “Blind timing and carrier synchronisation in distributed multiple input multiple output communication systems,” IET Commun., vol. 5, no. 7, pp. 1028–1037, 2011.

[18] A. Goldsmith. *Wireless Communications*, Cambridge university press, 2005.

[19] Z. Zhang, W. Zhang, and C. Tellambura, “MIMO-OFDM Channel Estimation in the Presence of Frequency Offsets,” *IEEE Trans. Wireless Commun.*, vol.7, no. 6, pp.2329-2339, June 2008.

[20] Johan Skld Erik Dahlman, Stefan Parkvall. *4G: LTE/LTE-Advanced for Mobile Broadband*, chapter 3. Academic Press, 2013.

[21] Markku Pukkila, “Channel Estimation Modeling,” *Postgraduate Course in Radiocommunications*, 2000.

[22] Wei Zhang. *Channel and frequency offset estimation for OFDM-based systems*. PHD thesis, University of Alberta, 2011.

[23] M. Schellmann and V. Jungnickel, “Effects of multiple users’ CFOs in OFDM-SDMA up-link – an interference model,” *IEEE International Conference on Communications*, June 2006, pp. 4642-4647.

[24] *Synchronization for OFDM Systems*. EIT 140, Lund University.